https://dx.doi.org/10.1016/j.jsv.2022.116754

A nonlinearity-sensitive approach for detection of "breathing" cracks relying on energy modulation effect

Maosen Cao[a,b,c], Qitian Lu[a,b], Zhongqing Su[d], Maciej Radzieński[e],

Wei Xu[a,b,c,*], Wiesław Ostachowicz[e]

[a] Department of Engineering Mechanics, Hohai University, Nanjing 210098, People's Republic of China

[b] Jiangsu Province Wind Power Structural Engineering Research Center, Hohai University, Nanjing 210098, People's Republic of China

[c] Jiangxi Provincial Key Laboratory of Environmental Geotechnical Engineering and Disaster Control, Jiangxi University of Science and Technology, Ganzhou 341000, People's Republic of China

[d] Department of Mechanical Engineering, The Hong Kong Polytechnic University, Hung Hom, Kowloon, Hong Kong, People's Republic of China

[e] Institute of Fluid-Flow Machinery, Polish Academy of Sciences, Gdańsk 80-231, Poland

[*]Corresponding author.
E-mail address:
wxu@hhu.edu.cn (W. Xu)

Abstract: For a cracked structural component under a single-tone harmonic excitation, the opening-closing motion of the “breathing” crack can lead to higher harmonics in its steady-state responses, which can be efficient indicators for the detection of the crack. Nevertheless, when the opening-closing motion of a “breathing” crack is slight, higher harmonics can become barely visible in frequency spectra and seem to be hidden. As a consequence, the crack can hardly be detected by such hidden higher harmonics. Addressing this problem, this study proposes a nonlinearity-sensitive approach for the detection of “breathing” cracks. In particular, a novel phenomenon of energy modulation effect (EME) is reported, based on which a new concept of quadratic TKE (Q-TKE) is formulated. Hidden higher harmonics can be considerably enhanced in Q-TKEs, such that “breathing” cracks can be readily detected. A physical insight into the mechanism of the EME is provided. The approach is numerically verified using the finite element method and experimentally validated through non-contact laser measurement. The results suggest that hidden higher harmonics can be considerably enhanced in the Q-TKEs and become sensitive indicators to manifest the occurrence of the cracks, suitable for the detection of initial fatigue cracks.

***Keywords*:** “breathing” crack; higher harmonics; energy modulation effect; quadratic Teager-Kaiser energy; non-contact laser measurement

1. Introduction

Fatigue cracks can occur in structural components under long-term cyclic loads [1]. Such fatigue cracks can open and close during tension and compression, referred to as "breathing" cracks.

In the recent three decades, a great amount of research has been focused on modeling "breathing" cracks to simulate their opening-closing motions during vibration. In the early research, cracked structures were simplified as oscillators with single degree-of-freedoms (DOFs) [2-11]. Extended to cracked structures with multiple DOFs, periodical changes in crack locations were introduced into dynamic stiffness matrices to model "breathing" cracks [12-19]. For continuous cracked beams with infinite DOFs, "breathing" cracks were modeled in analytical manners [20-25].

Due to opening-closing motions of "breathing" cracks, higher harmonics generated by the cracks can appear at successive multiples of the excitation frequencies in frequency spectra [26,27]. These higher harmonics can be efficient indicators for the detection of "breathing" cracks in the field of nondestructive testing [28-36]. The representative studies are as follows. Hu *et al.* [28] investigated the nonlinear vibro-acoustic modulation technique for damage detection in metallic structures using instantaneous amplitudes and frequencies. Semperlotti *et al.* [29] proposed a method for localization of "breathing" cracks using phase differences of higher harmonics. The method was numerically verified by the finite element (FE) method. Further, the method was enhanced with combination tones and experimentally validated [30]. Broda *et al.* [31] investigated nonlinearities of longitudinal vibration of beams with "breathing" cracks. The results demonstrated that nonlinearities in cracked beams were particularly strong in the vicinity of cracks. Wang *et al.* [32] investigated the underlying mechanism of interaction between guided ultrasonic waves and "breathing" cracks. Contact

acoustic nonlinearity manifests unique scattering patterns associated with the crack slant, which can be used for orientating cracks. Asnaashari *et al.* [33] proposed a method for the detection and localization of "breathing" cracks using residual operating deflection shapes (ODSs), which are the differences between normalized ODSs at first and higher harmonics. Lu *et al.* [34] proposed a method for "breathing" crack localization using crack-induced local shape distortions in higher harmonic characteristic deflection shapes. Xu *et al.* [35] proposed a new concept of nonlinear pseudo-force, which was formulated from ODSs at higher harmonics. The concept can be used to locate cracks and expound the mechanism for generating higher harmonics by "breathing" cracks. Cui *et al.* [36] employed bispectrum analysis for the detection of "breathing" cracks by investigating the nonlinear dynamic characteristics of cracked beams.

Although higher harmonics can manifest the occurrence of "breathing" cracks, they are usually much weaker than the first harmonics when the opening-closing motions of the "breathing" cracks are slight. In these situations, higher harmonics are overshadowed by the first harmonics, which seem to be hidden. As a consequence, the crack can barely be detected by such hidden higher harmonics. Addressing this problem, this study proposes a nonlinearity-sensitive approach for the detection of "breathing" cracks. In particular, a new phenomenon of energy modulation effect (EME) is reported, based on which a new concept of quadratic TKE (Q-TKE) is formulated. Hidden higher harmonics can be considerably enhanced in Q-TKEs, such that "breathing" cracks can be readily detected.

The rest of the paper is organized as follows. Section 2 reports the new phenomenon of EME and provides a physical insight into its mechanism for enhancing higher harmonics. On the basis of the EME, a new concept of Q-TKE is formulated,

hidden higher harmonics in which can be considerably enhanced for the detection of "breathing" cracks. Section 3 numerically verifies the capability of the approach for the detection of "breathing" cracks using the FE method. Section 4 experimentally validates the applicability of the approach on a steel beam that bears a fatigue "breathing" crack, whose steady-state velocity responses under single-tone harmonic excitations are acquired through non-contact vibration measurement using a Doppler laser vibrometer (DLV). The numerical and experimental results suggest that the approach is capable of detecting hidden higher harmonics, which can improve the efficiency and sensitivity of existing approaches of fatigue crack detection relying on higher harmonics. Section 5 presents concluding remarks.

2. EME for enhancing hidden higher harmonics

Consider a cracked structural component that is under a single-tone harmonic excitation at ω_f. Due to the opening-closing motion of the "breathing" crack, its steady-state response $f(t)$ consists of multiple harmonics [27]:

$$f(t) = \sum_{m=1} A_m \cos(\omega_m t + \phi_m), \tag{1}$$

where t is time and A_m, ω_m, and ϕ_m are the amplitude, angular frequency, and phase of the *m*th harmonic, respectively. Note that the response can be displacement, velocity, or acceleration. Harmonics in the frequency spectrum are distributed at successive multiples of the excitation frequency, *i.e.*, $\omega_m = m\omega_f$. In the situation that the opening-closing motion of the "breathing" crack is slight, the generated higher harmonics are much less pronounced compared to the first harmonics, leading to $A_m \ll A_1$. In this study, the Teager-Kaiser energy (TKE) [37] is used to measure the pointwise energy of $f(t)$, denoted as $E(t)$:

$$E(t)=\psi(f(t))=(\frac{\mathrm{d}f(t)}{\mathrm{d}t})^2-f(t)\frac{\mathrm{d}^2 f(t)}{\mathrm{d}t^2}, \tag{2}$$

where $\psi(\cdot)$ denotes the TKE operator. Note that $\psi(\cdot)$ is further extended to $\psi_c(\cdot)$ for calculation of the TKE between two functions [38]:

$$\psi_c(f(t),g(t))=\frac{\mathrm{d}f(t)}{\mathrm{d}t}\frac{\mathrm{d}g(t)}{\mathrm{d}t}-f(t)\frac{\mathrm{d}^2 g(t)}{\mathrm{d}t^2}, \tag{3}$$

By substituting Eq. (1) into Eq. (2), $E(t)$ can be re-written as per the property of the TKE operator [38] (see Appendix A for details):

$$E(t)=\psi(f(t))=\sum_{m=1}\psi(A_m\cos(\omega_m t+\phi_m))+\sum_{\substack{m,n=1\\ m\neq n}}\psi_c(A_m\cos(\omega_m t+\phi_m),A_n\cos(\omega_n t+\phi_n)). \tag{4}$$

In Eq. (4), $\psi(A_m\cos(\omega_m t+\phi_m))$ is a constant related to the amplitude and frequency of the *m*th harmonic [39]:

$$\psi(A_m\cos(\omega_m t+\phi_m))=A_m^2\omega_m^2, \tag{5}$$

and $\psi_c(A_m\cos(\omega_m t+\phi_m),A_n\cos(\omega_n t+\phi_n))$ can be expressed as

$$\begin{aligned}\psi_c[A_m\cos(\omega_m t+\phi_m),A_n\cos(\omega_n t+\phi_n)] &= A_m A_n\omega_m\omega_n\sin(\omega_m t+\phi_m)\sin(\omega_n t+\phi_n)\\ &\quad + A_m A_n\omega_n^2\cos(\omega_m t+\phi_m)\cos(\omega_n t+\phi_n)\\ &= \frac{1}{2}A_m A_n(\alpha_{mn}+\beta_{mn}),\end{aligned} \tag{6}$$

where α_{mn} and β_{mn} are

$$\alpha_{mn}=\omega_m\omega_n(\cos((\omega_m-\omega_n)t+\phi_m-\phi_n)-\cos((\omega_m+\omega_n)t+\phi_m+\phi_n)), \tag{7}$$

$$\beta_{mn}=\omega_n^2(\cos((\omega_m-\omega_n)t+\phi_m-\phi_n)+\cos((\omega_m+\omega_n)t+\phi_m+\phi_n)). \tag{8}$$

Equation (6) indicates that the EME occurs between any two components of harmonics in $f(t)$: the modulation between harmonics at ω_m and ω_1 ($n=1$) generates the energy component of $E(t)$ at $\omega_m\mp\omega_1$ ($m=2,3...$), whose amplitudes are associated with the amplitude of the first harmonic A_1 ($A_1\ll A_m$) and the frequency of the *m*th

harmonic ω_m (ω_m=$m\omega_1$). As a consequence, compared to steady-state responses, the amplitude ratios of the mth harmonics to the first harmonics largely increase in their TKE due to the EME. In light of this effect, the concept of the Q-TKE is further proposed:

$$E_2(t)=\psi(E(t))=\psi(\psi(f(t))). \tag{9}$$

In the Q-TKE, higher harmonics in $E(t)$ can be further enhanced with largely increased amplitudes. Hence, hidden higher harmonics in $f(t)$ can become noticeable and easy to identify, which is beneficial to the detection of the "breathing" crack. Note that for a discretized $f(t)$, discrete forms of the TKE and Q-TKE can be expressed as, respectively [37]

$$E[t]=\psi[f[t]]=f^2[t]-f[t-1]f[t+1], \tag{10}$$

$$\begin{aligned} E_2[t]=\psi[\psi[f[t]]]=&(f^2[t]-f[t-1]f[t+1])^2 \\ &-(f^2[t-1]-f[t-2]f[t])(f^2[t+1]-f[t]f[t+2]). \end{aligned} \tag{11}$$

Thereby, on the basis of the EME, a nonlinearity-sensitive approach is proposed, by which the hidden harmonics can be considerably enhanced in Q-TKEs and become sensitive indicators for the detection of "breathing" cracks.

3. Numerical verification

3.1 Numerical model

To verify the EME reported in Section 2, a steel cantilever beam with a "breathing" crack is considered a numerical specimen. A numerical model of the beam is shown in Fig. 1 with dimensions in millimeters. The length, width, and thickness of the beam are 400 mm, 10 mm, and 20 mm, respectively. One end of the beam is fixed, spanning 20 mm in length from the edge of the fixed end. The beam is modeled by the FE software ANSYS with eight-node hexahedral elements whose dimensions are 10 mm × 2.5 mm

× 2 mm in the length, width, and thickness directions, respectively. The elastic modulus, Poisson's ratio, and material density are 150 GPa, 0.27, and 7800 Kgm^{-3}, respectively. A through-width perpendicular crack is modeled by inserting non-thickness interfaces between crack interfaces, on which the coincident nodes in adjacent but separated elements are distributed. Natural frequencies and mode shapes can be calculated by the modal analysis module in ANSYS. Note that only flexural modes are considered in this study. Figure 2 shows the first mode shape of the beam with a zoomed-in view of the crack, on whose interfaces nodes are marked in different colors (yellow and red) for distinction. To simulate the "breathing" behavior of the crack, contact elements are introduced between the two crack interfaces, which are defined as contact and target surfaces. The penalty algorithm in ANSYS is used to generate contact forces by virtual springs between the crack interfaces, by which the crack interfaces are allowed to separate but not to penetrate into each other. For this lightly-damped beam, the damping ratio $\xi = 0.1$ is considered according to the Rayleigh damping:

$$\xi = \frac{\alpha}{2\omega} + \frac{\beta\omega}{2}, \tag{12}$$

where α and β are mass and stiffness damping parameters, respectively.

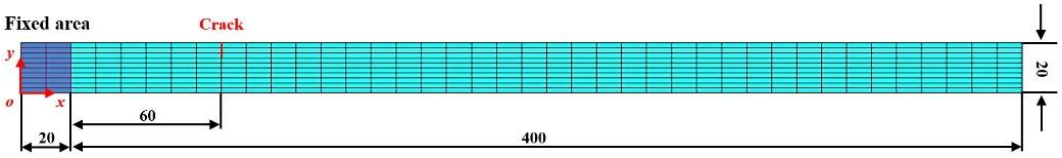

Fig. 1 Numerical model of the steel beam with the crack (dimensions in millimeters).

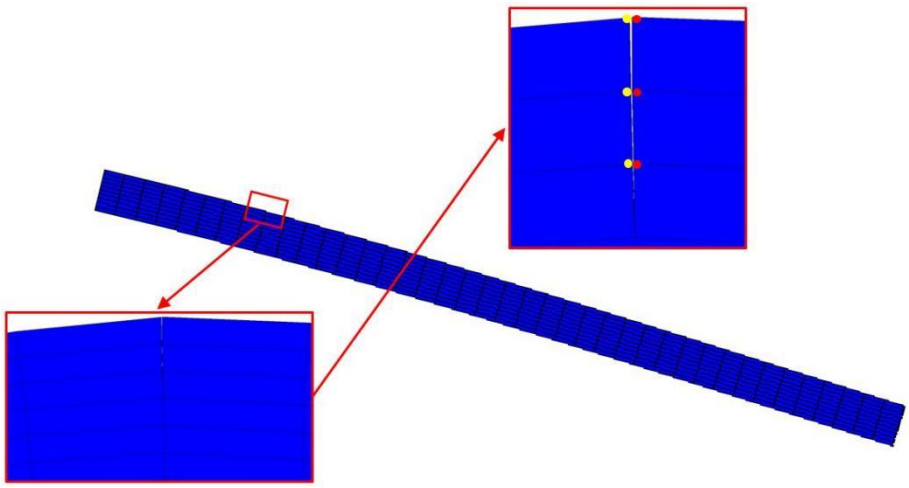

Fig. 2 The first mode shape of the cracked beam with a zoomed-in view of the crack (nodes on two crack interfaces are marked by red and yellow dots).

A concentrated harmonic force is applied on the beam near its fixed end (30 mm away from the edge of the fixed end), by which single-tone harmonic excitations are generated in the transverse direction. Simultaneously, steady-state transverse velocity responses are extracted from the node located at 10 mm from the free end of the beam. It is noteworthy that the location of the measurement point is selected close to the free end of the beam for generality and repeatability; on the other hand, the node effect can be avoided as transverse displacements vanish in the locations of nodes. Forty points are sampled in each period of the steady-state response. As the beam is lightly damped, it can be excited at arbitrary frequencies, including flexural natural frequencies. Steady-state displacement or acceleration responses can also be used for crack detection. In this study, the velocity responses are directly measured using the DLV in the experiment. Therefore, only velocity responses are used in the numerical simulation to keep consistent with the experiment.

3.2 Numerical results

3.2.1 Detection of "breathing" crack

To verify the capability of the approach for detecting "breathing" cracks subject to excitations at arbitrary frequencies, the beam is excited at resonance or non-resonance frequencies (ω_1, $1/2\omega_1$, and $1/3\omega_1$ with ω_1 denoting the first natural frequency of the beam), denoted as numerical Scenarios I, II, and III, respectively (listed in Table 1). In these scenarios, the crack is located at $x = 80$ mm (dimensionless location $\zeta = 0.2$) with a depth of $h = 3$ mm (dimensionless depth $\xi = 0.3$). To ensure the "breathing" crack can totally open and close during vibration for all numerical scenarios, the amplitudes of the excitation forces are set to be 100 N after trials. For numerical Scenarios I, II, and III, the time histories of the velocity responses with 1000 sampling points are shown in Figs. 3(a), (c), and (e), respectively. By the fast Fourier transform (FFT), corresponding frequency spectra of the velocity responses are calculated and shown in Figs. 3(b), (d), and (f). It can be seen that higher harmonics generated by the crack are almost invisible in each frequency spectrum. To enhance the higher harmonics, the Q-TKEs of the velocity responses for numerical Scenarios I, II, and III are obtained by Eq. (11), corresponding frequency spectra of which are calculated and shown in Figs. 4(a), (b), and (c) for Scenarios I, II, and III, respectively. It can be seen from Fig. 4 that peaks appear at the double, triple, and quadruple excitation frequencies to indicate the 2nd, 3rd, and 4th higher harmonics, respectively, whereby the occurrence of the crack can be evidently manifested.

Table 1. Numerical Scenarios I-VIII.

Scenario	I	II	III	IV	V	VI	VII	VIII
Excitation frequency [Hz]	ω_1	$1/2\omega_1$	$1/3\omega_1$	ω_1	ω_1	ω_1	ω_1	ω_1
Crack depth ξ	0.3	0.3	0.3	0.2	0.1	0.3	0.3	0.3
Crack location ζ	0.2	0.2	0.2	0.2	0.2	0.4	0.6	0.8

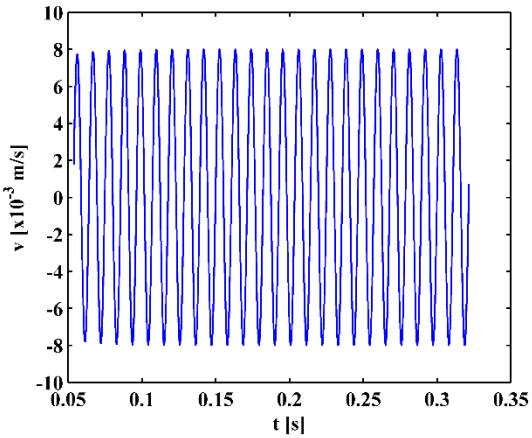

(a)

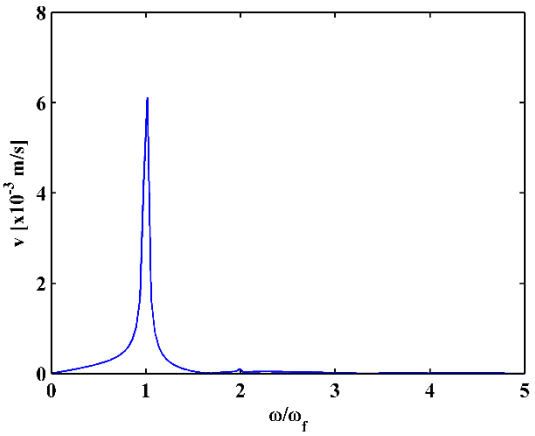

(b)

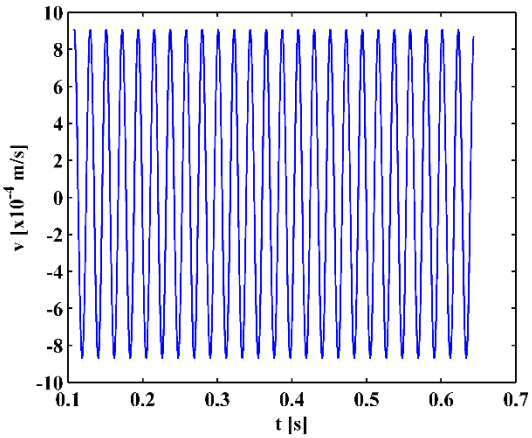

(c)

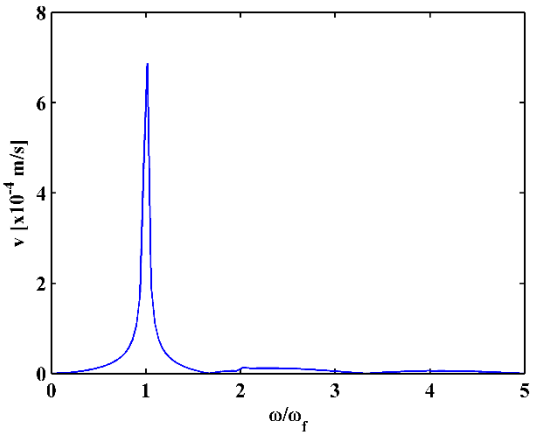

(d)

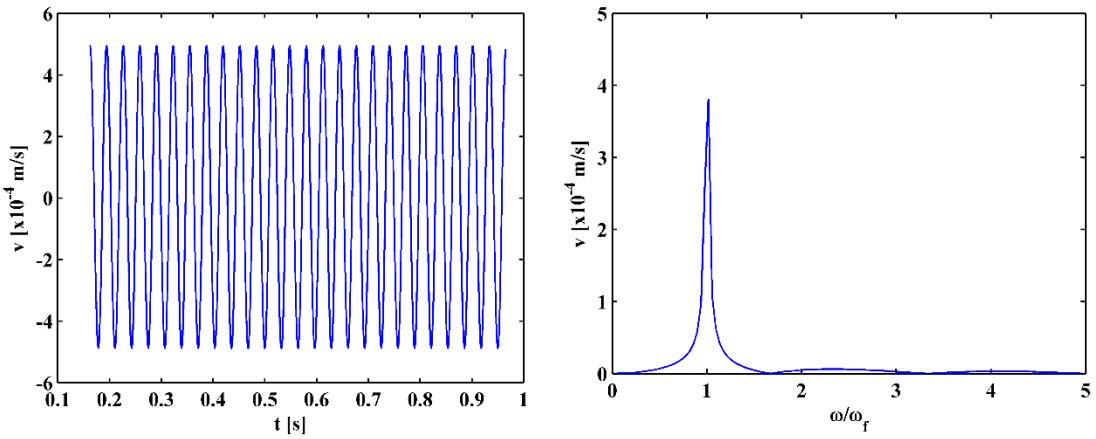

(e) (f)

Fig. 3 Time histories of the velocity responses for numerical Scenarios (a) I, (c) II, and (e) III and their frequency spectra (b) I, (d) II, and (f) III.

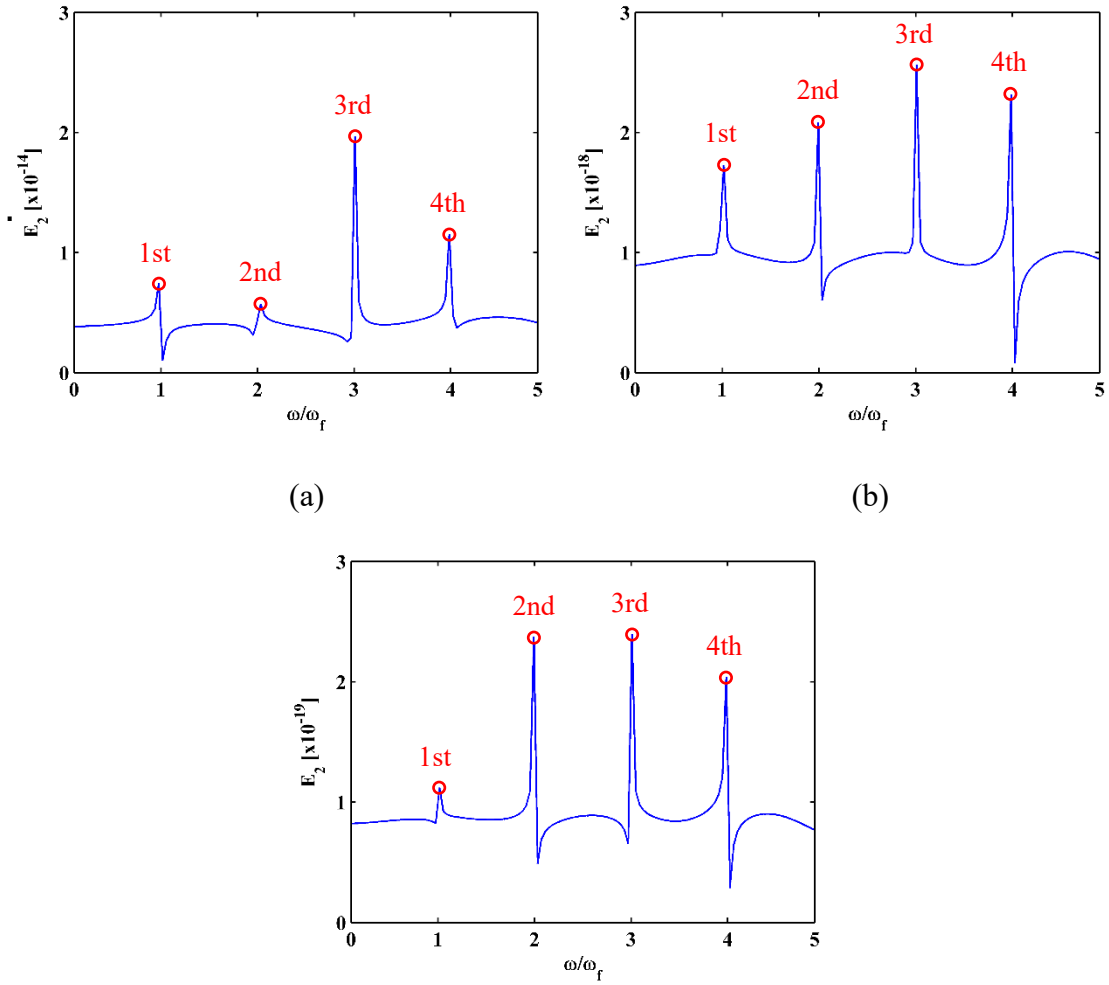

(a) (b)

(c)

Fig. 4 Frequency spectra of Q-TKEs for numerical Scenarios (a) I, (b) II, and (c) III.

To investigate the sensitivity of the approach to crack depth, numerical Scenarios IV with $\xi = 0.2$ and V with $\xi = 0.1$ are considered for comparison with numerical Scenarios I with $\xi = 0.3$ (listed in Table 1). Time histories and frequency spectra for the three scenarios are shown in Figs. 5(a) and (b), respectively. It can be seen that the steady-state responses are dominated by linear vibration, whereas the second harmonics are barely visible due to weak vibration caused by the crack, as shown in Fig. 5(b). On the other hand, amplitudes of the steady-state responses slightly increase with the crack depth due to the decrease in bending stiffness in the crack location. In contrast, as shown in Fig. 6(a), characteristics of nonlinear vibration can be clearly observed in the frequency spectra of Q-TKEs, in which amplitudes of higher harmonics increase with crack depths. As the Q-TKE for numerical Scenario V is largely overshadowed by the Q-TKEs for numerical Scenarios I and IV, the Q-TKE for numerical Scenario V is shown in Fig. 6(b) to display its details.

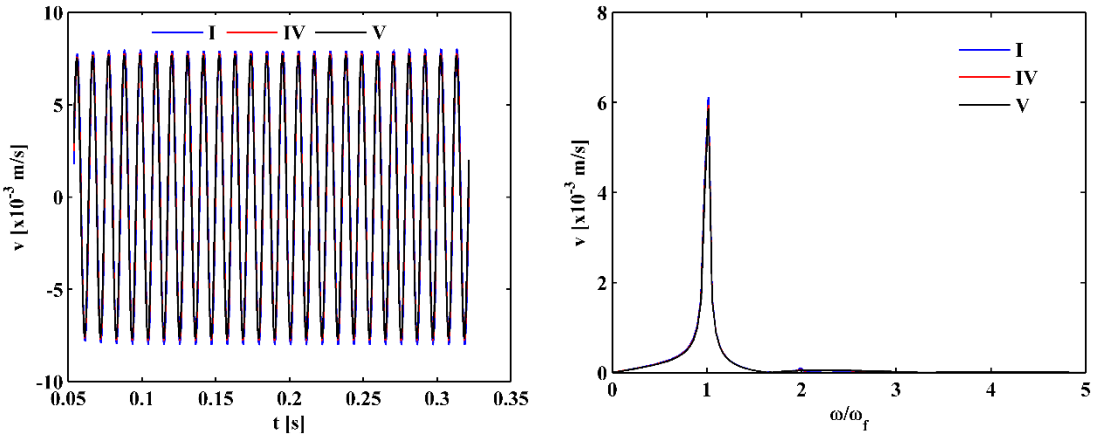

(a) (b)

Fig. 5 (a) Time histories and (b) frequency spectra of velocity responses for numerical Scenarios I, IV, and V.

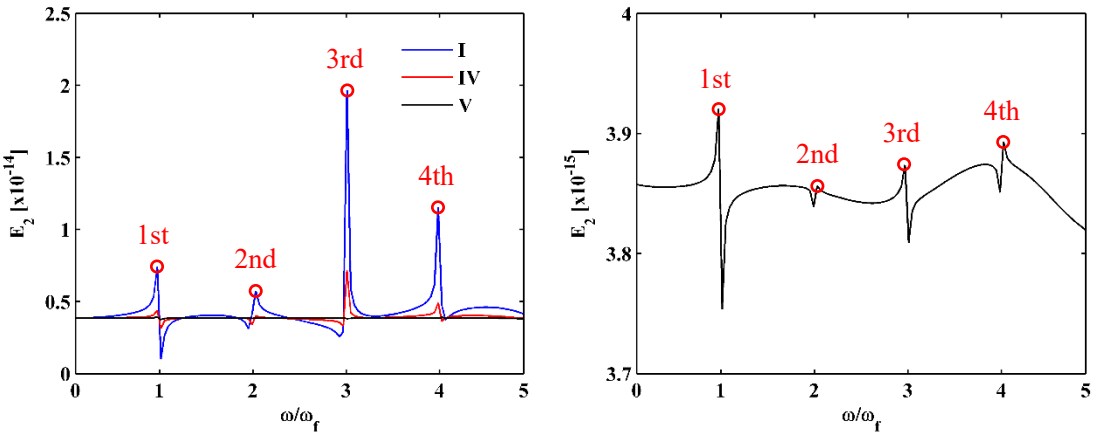

(a) (b)

Fig. 6 Frequency spectra of Q-TKEs for (a) numerical Scenarios I, IV, and V, and for (b) numerical Scenario V.

The results suggest that hidden higher harmonics can be considerably enhanced in the Q-TKEs and become sensitive indicators to manifest the occurrence of the cracks, such that the cracks can be readily detected, suitable for the detection of initial fatigue cracks.

3.2.2 Effects of crack locations on the approach

To investigate the effects of crack locations on the approach, numerical Scenarios VI with $\zeta = 0.4$, VII with $\zeta = 0.6$, and VIII with $\zeta = 0.8$ are considered for comparison with numerical Scenarios I with $\zeta = 0.2$ (listed in Table 1). Time histories and frequency spectra for the four scenarios are shown in Figs. 7(a) and (b), respectively. It can be seen that linear vibration dominates the steady-state responses; on the other hand, amplitudes of the steady-state responses largely increase with the crack locations when crack moves towards its free end.

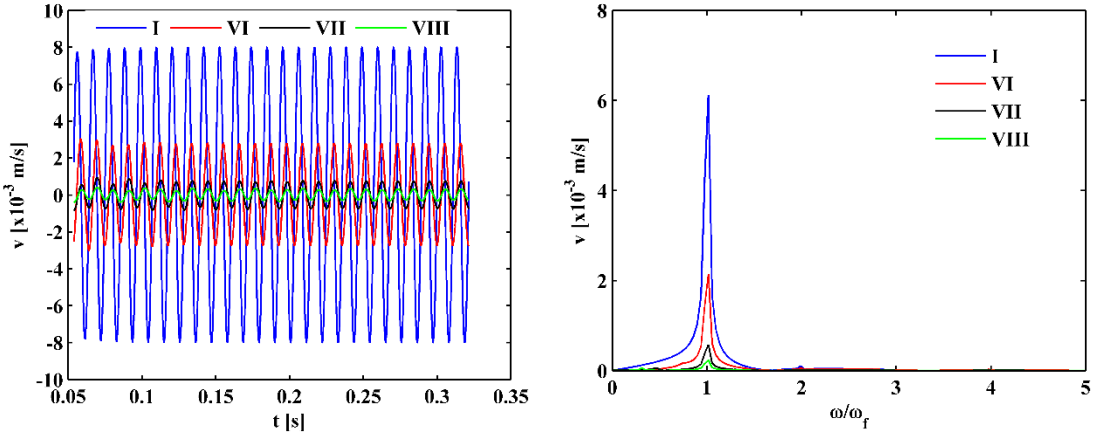

Fig. 7 (a) Time histories and (b) frequency spectra of velocity responses for numerical Scenarios I, VI, VII, and VIII.

It is noteworthy that small random uncertainties can occur during the numerical simulation and cause perturbation in steady-state responses, leading to interference in Q-TKEs. As a consequence, steady-state responses with smaller amplitudes are susceptible to such interference. As shown in Fig. 8, although higher harmonics appear in the Q-TKEs, their magnitudes decrease and become increasingly unsmooth because the TKE operator can amplify small random uncertainties involved in signals [37, 39]. In particular, interference peaks appear in Fig. 8(c) and largely increase in Fig. 8(d). Such fake peaks can be mistaken for the crack-caused peaks. In Fig. 8(c), the first harmonic is ambiguous; and in Fig. 8(d), the first and third harmonics can hardly be identified. Thereby, excitation frequencies for a cracked structural component are suggested to be selected near its fundamental frequencies for large vibration amplitudes; meanwhile, excitation and measurement points need to be properly selected to acquire large amplitudes of vibration responses.

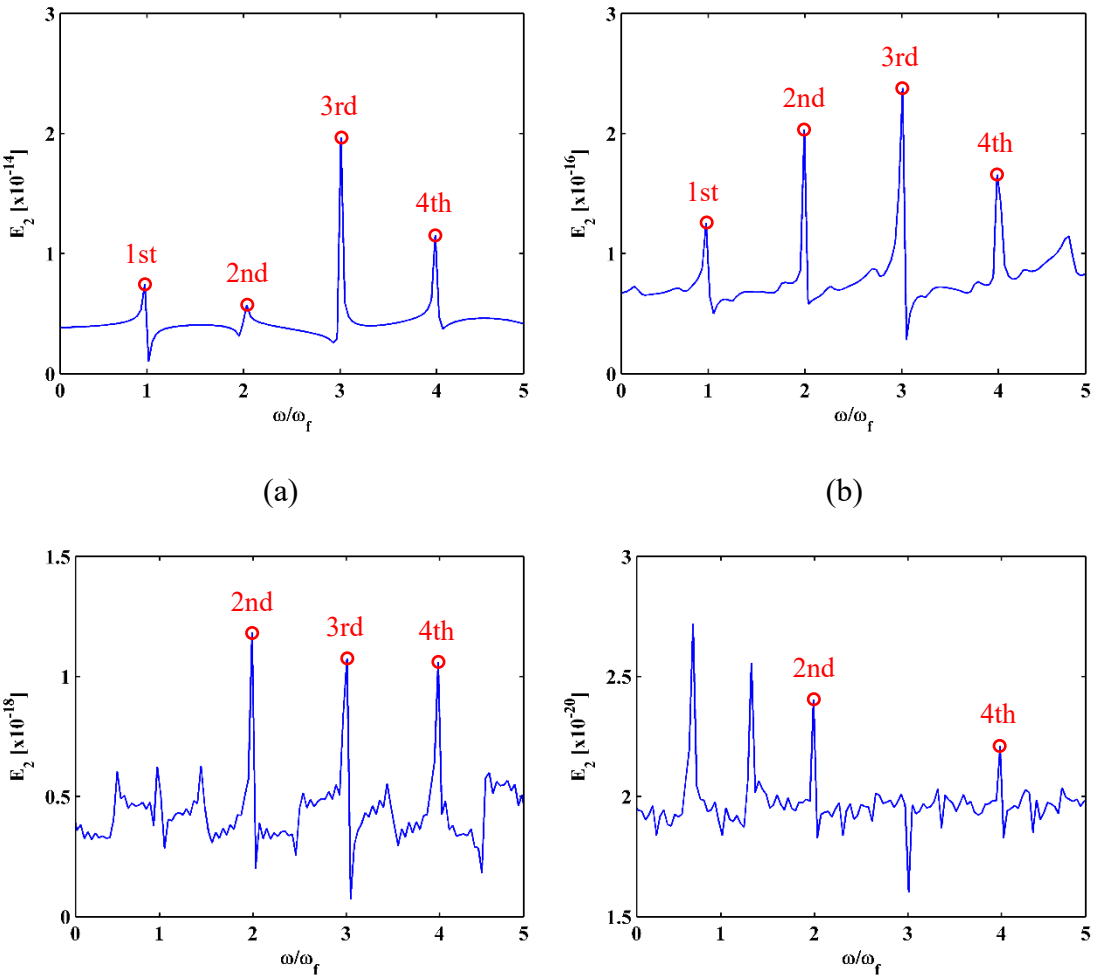

Fig. 8 Frequency spectra of the Q-TKEs for numerical Scenarios (a) I, (b) VI, (c) VII, and (d) VIII.

3.2.3 Robustness of the approach against noise interference

In practical scenarios, noise components can inevitably be contained in steady-state responses of structural components. To investigate the robustness of the approach against noise interference, different noise levels are considered for numerical Scenario I. Frequency spectra of the Q-TKEs associated with noise levels of 1%, 3%, 5%, and 10% are shown in Figs. 9(a), (b), (c), and (d), respectively. It can be seen that noise-caused interference peaks increase with noise levels. For noise level of 1% (Fig. 9(a)), interference peaks appear but the peaks of harmonics can still be evidently identified; for the noise level of 3% (Fig. 9(b)), interference peaks increase to obscure the first

harmonic; for the noise level of 5% (Fig. 9(c)), interference peaks become intense, making the first and fourth harmonics ambiguous; for the noise level of 10% (Fig. 9(d)), noise interference dominates the Q-TKE, only the second harmonic can be clearly identified. Similar to the situation of random uncertainties, such fake peaks caused by noise can be mistaken for the crack-caused peaks. Therefore, de-noising is suggested for practical applications of the Q-TKE for in-service structural components.

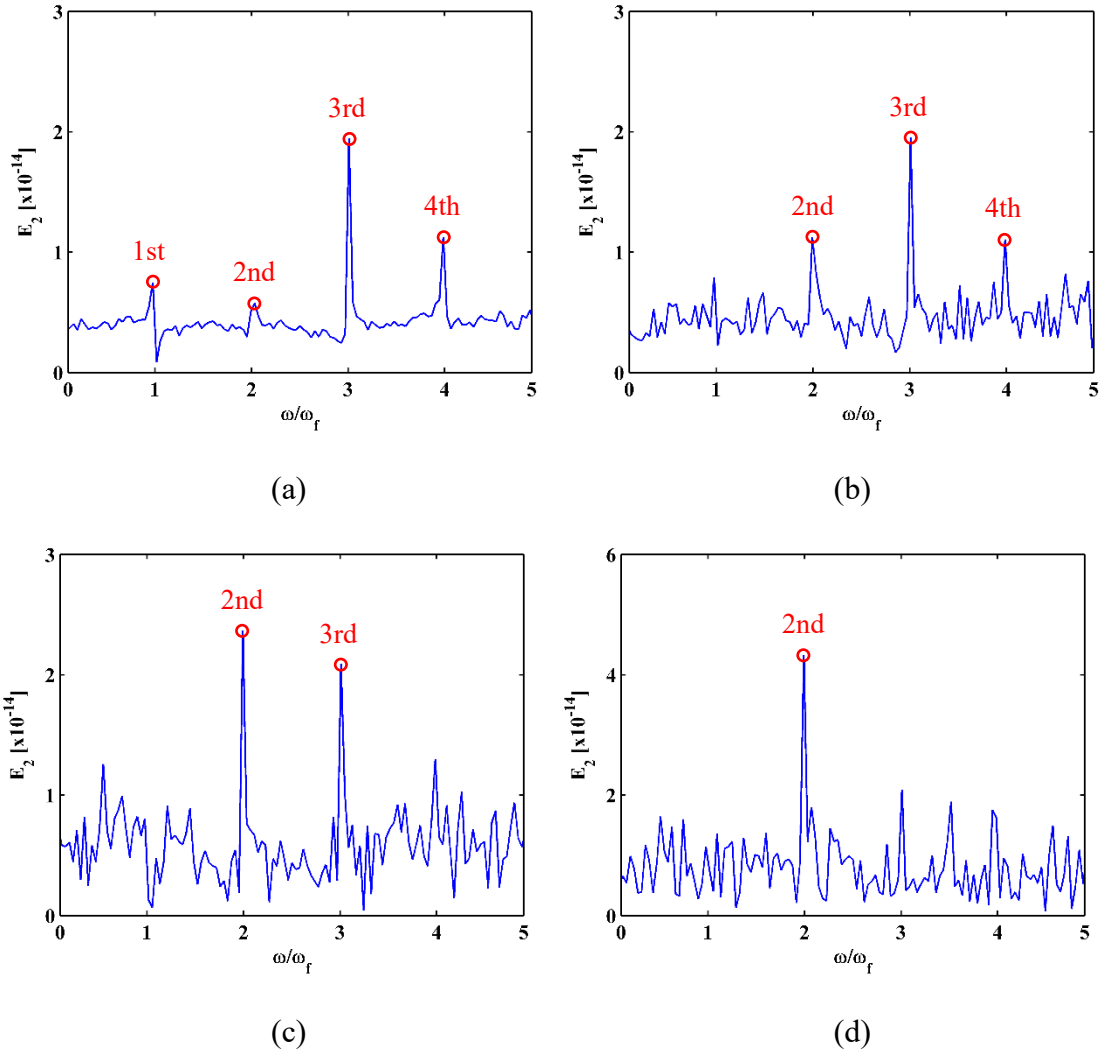

Fig. 9 Frequency spectra of the Q-TKEs for numerical Scenario I with noise levels of (a) 1%, (b) 3%, (c) 5%, and (d) 10%.

4. Experimental validation

4.1 Experimental specimen and setup

To validate the applicability of the EME for the detection of "breathing" cracks, a steel cracked beam is taken as an experimental specimen, whose dimensions are 400 mm × 10 mm × 20 mm in length, width, and thickness, respectively. A sketch of the experimental specimen is shown in Fig. 10, with its dimensions in millimeters. One end of the beam is fixed by a vice, spanning 18 mm in length from the edge of the fixed end. A through-width V-shaped notch was manufactured in the beam, 92 mm away from the edge of the fixed end. The notch is 1 mm in depth, in the tip of which a fatigue crack initiates and propagates to 5 mm in depth after fatigue loadings.

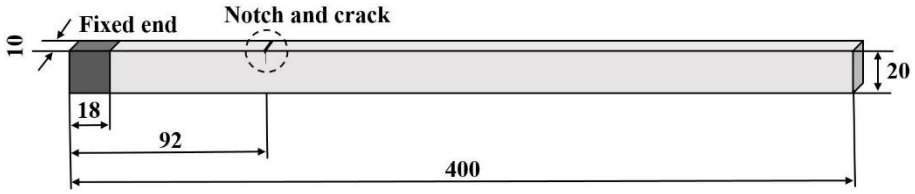

Fig. 10 Sketch of the steel beam with a notch and a fatigue crack (dimensions in millimeters).

An electromechanical shaker is attached to the intact surface (400 mm in length and 10 mm in width) of the beam, 30 mm away from the edge of the fixed end. An arbitrary waveform generator controls the shaker to generate single-tone harmonic excitations in the transverse direction. The excitation force amplitudes are proportional to the output voltage amplitudes in the arbitrary waveform generator. The first natural frequency ω_1 of the beam is 70.63 Hz. The DLV is used to acquire the steady-state transverse velocity responses from the measurement point, which is located 4 mm away from the free end of the beam. The sampling frequency is 12.8 kHz. The schematic of vibration measurement is shown in Fig. 11, where the notch and crack are shown in a zoomed-in view. Note that the displacement and acceleration responses can be exported from velocity responses by means of integration and differentiation, respectively.

Although steady-state displacement or acceleration responses can also be used for crack detection, only steady-state velocity responses are used in this study because they are directly measured using the DLV.

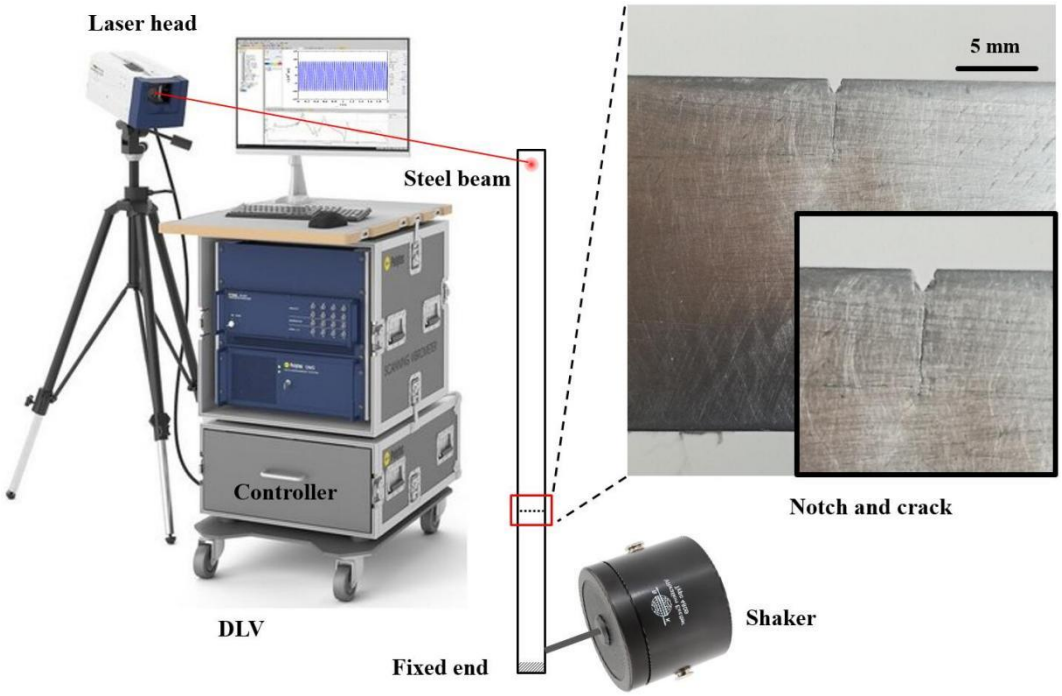

Fig. 11 Schematic of vibration measurement with a zoomed-in view of the notch and crack.

4.2 Experimental results

4.2.1 Detection of "breathing" fatigue crack

Experimental Scenarios I, II, and III associated with different excitation frequencies (listed in Table 2) are considered for experimental validation. To ensure that the crack fully opens and closes during vibration, the input voltage in the shaker is set to be 1 V after trials. For Scenarios I, II, and III, the beam is excited at ω_1, $1/2\omega_1$, and $1/3\omega_1$, whose time histories of the steady-state velocity responses in one second are shown in Figs. 12(a), (c), and (e), respectively. By the FFT, corresponding frequency spectra are obtained and shown in Figs. 12(b), (d), and (f), where higher harmonics appear to manifest the occurrence of the crack. Thereby, the crack can be readily detected by

higher harmonics due to strong nonlinearity of vibration, which is produced when the crack fully opens and closes subject to the excitations with large amplitudes.

Table 2 Experimental Scenarios I-VIII.

Scenario	**I**	**II**	**III**	**IV**	**V**	**VI**	**VII**	**VIII**
Excitation frequency [Hz]	ω_1	$1/2\omega_1$	$1/3\omega_1$	ω_1	$1/2\omega_1$	$1/3\omega_1$	ω_2	ω_3
Excitation voltage [V]	1	1	1	0.125	0.125	0.125	0.125	0.125

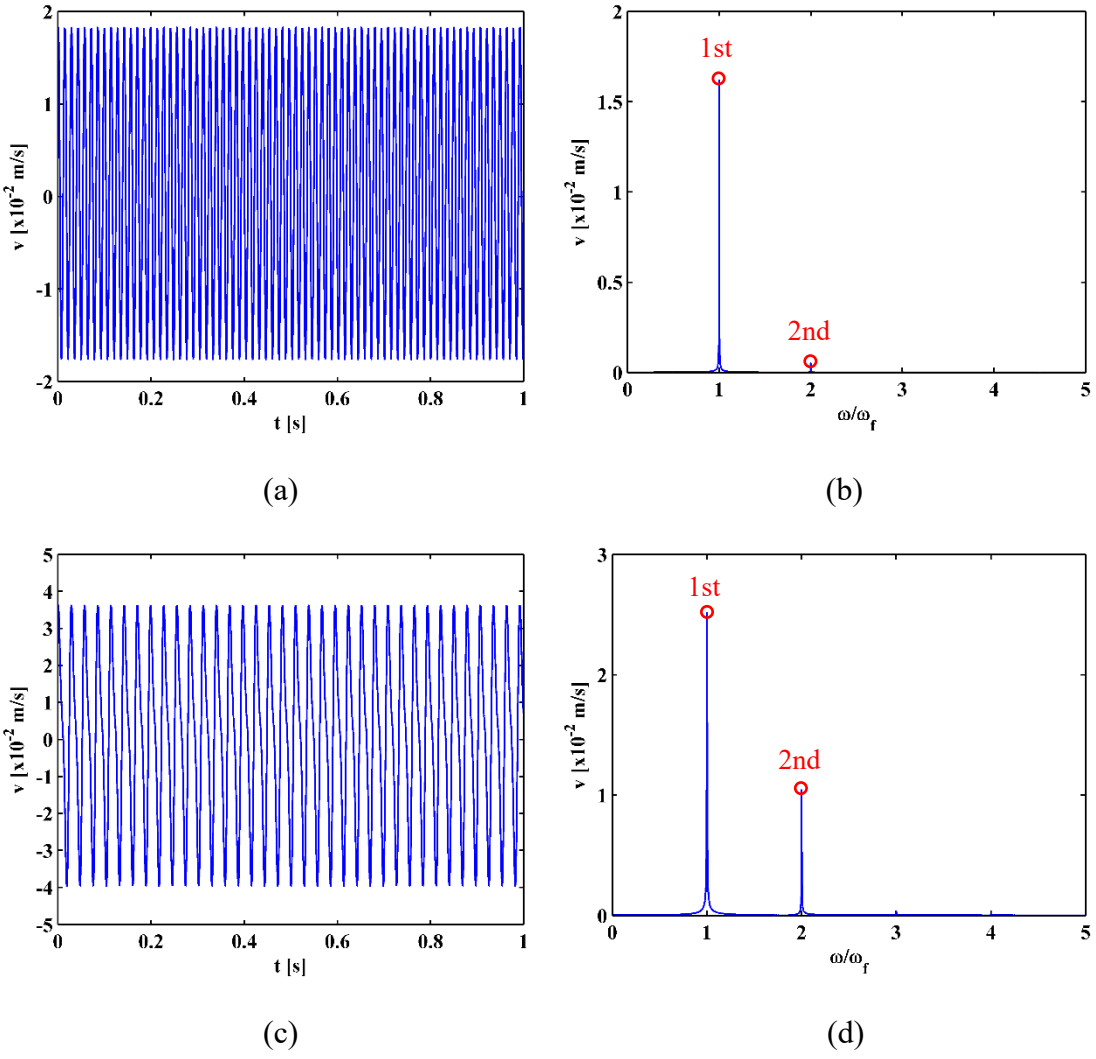

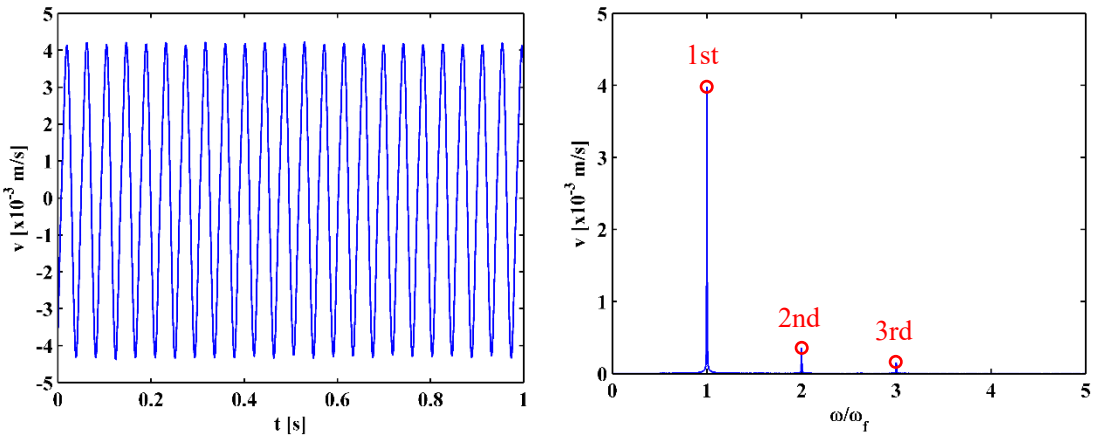

(e) (f)

Fig. 12 Frequency spectra of velocity responses for Scenarios (a) I, (c) II, and (e) III and Q-TKEs for Scenarios (b) I, (d) II, and (f) III.

4.2.2 Detection of partially-open "breathing" fatigue crack

For cracked structural components subject to excitations with small amplitudes, higher harmonics generated by the "breathing" cracks can be too weak to indicate the cracks due to the partially-open motions of the cracks. In this study, the proposed approach is utilized to detect such partially-open "breathing" cracks. To this end, experimental Scenarios IV, V, and VI with small excitation amplitudes are considered, associated with excitation frequencies of ω_1, $1/2\omega_1$, and $1/3\omega_1$, respectively (listed in Table 2). The input voltage in the shaker is set to be 0.125 V, such that the crack can fully close but practically open during vibration. For experimental Scenarios IV, V, and VI, the respective frequency spectra of the steady-state velocity responses and Q-TKEs are shown in Fig. 13. It can be seen from Figs. 13(a), (c), and (e) that only the first harmonics can be found when slight excitations apply because crack-caused weak nonlinear vibration can be negligible compared to the linear vibration [35]. To enhance the higher harmonics for the detection of the crack, the Q-TKEs of the steady-state velocity responses are calculated by Eq. (11), whose distributions in the frequency spectra are shown in Figs. 13(b), (d), and (f). It can be seen that the second, third, fourth

higher harmonics are considerably amplified, by which the crack can be evidently detected.

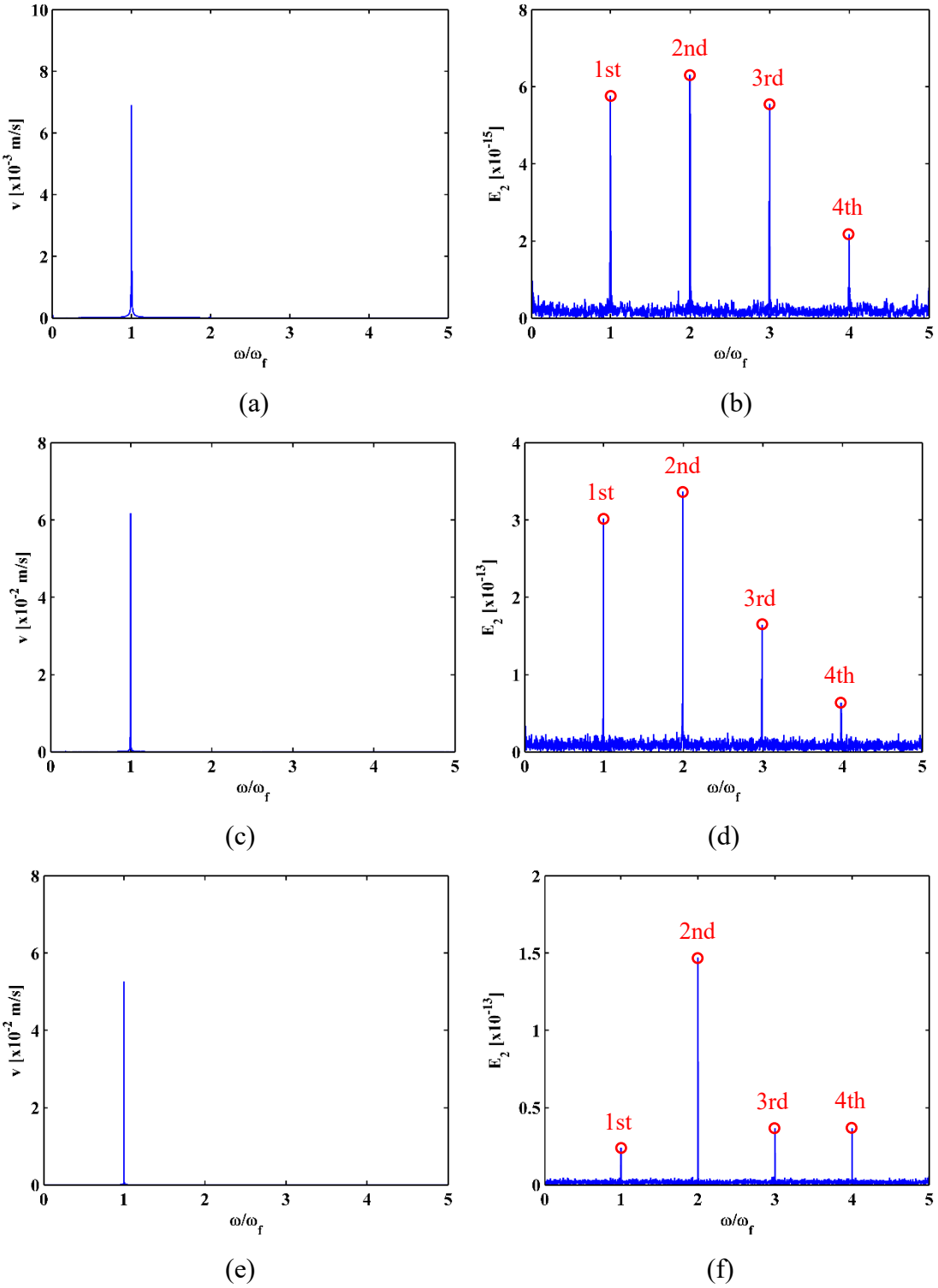

Fig. 13 Frequency spectra of velocity responses for Scenarios (a) VI, (c) V, and (e) VI and Q-TKEs for Scenarios (b) VI, (d) V, and (f) VI.

To prove the approach is sound and practical for arbitrary excitation frequencies, the second natural frequency ω_2 (688.70 Hz) and the third natural frequency ω_3 (1787.19 Hz) are used as excitation frequencies, denoted as experimental Scenarios VII and VIII, respectively (listed in Table 2). The input voltage in the shaker remains 0.125 V. As shown in Figs. 14(a) and (c), higher harmonics are almost invisible; in contrast, the corresponding Q-TKEs in Figs. 14(b) and (d) clearly show the crack-induced higher harmonics, whereby the crack can be evidently detected.

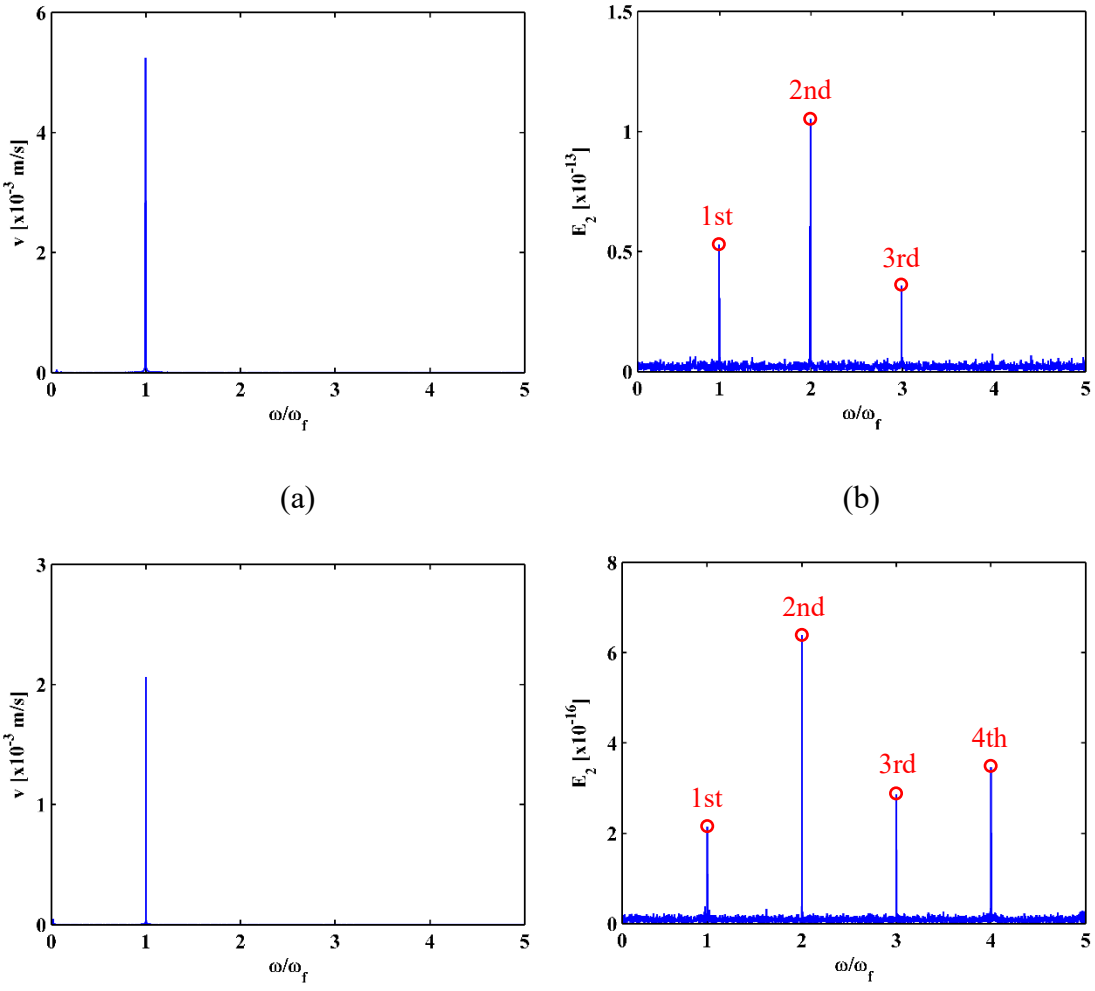

Fig. 14 Frequency spectra of velocity responses for Scenarios (a) VII and (c) VIII and Q-TKEs for Scenarios (b) VII and (d) VIII.

It is noteworthy that the EME reported in this study can also be used to detect other "breathing" damage such as weak bonds or delamination [40], higher harmonics generated by which can also be much less pronounced compared to the first harmonics. Besides higher harmonics, when vibro-acoustic excitations apply, side harmonics can be amplified as well for the detection of "breathing" damage [41].

5. Concluding remarks

Higher harmonics can be efficient indicators for the detection of "breathing" cracks in the field of nondestructive testing. Nevertheless, if the opening-closing motions of "breathing" cracks are slight, the cracks can be hardly detected by the hidden higher harmonics that are overshadowed by the first harmonics. Addressing this problem, this study proposes a nonlinearity-sensitive approach for the detection of "breathing" cracks. In particular, this study reports a novel phenomenon of EME, based on which a new concept of Q-TKE is formulated to considerably enhance hidden higher harmonics. This study provides a physical insight into the mechanism of the EME. The approach is numerically verified using the FE method and experimentally validated through the non-contact vibration measurement using the DLV. Some conclusions can be drawn as follows.

(1) The EME occurs between any two components of harmonics in steady-state responses of structural components bearing "breathing" cracks, by which amplitudes of higher harmonics are associated with amplitudes of the first harmonics and the frequency of higher harmonics. As a consequence, hidden higher harmonics can be considerably enhanced with noticeable amplitudes. Thereby, such enhanced higher harmonics can be sensitive indicators for the detection of "breathing" cracks, suitable for the detection of initial fatigue cracks.

(2) Random uncertainties can be amplified in Q-TKEs and cause fake peaks that can be mistaken for the crack-caused peaks. Steady-state responses with smaller amplitudes are susceptible to such interference. Thereby, excitation frequencies for a cracked structural component need to be selected near its fundamental frequencies for large vibration amplitudes; meanwhile, excitation and measurement points need to be properly selected to acquire large amplitudes of vibration responses.

(3) Similar to “breathing” cracks, other damage such as delamination can periodically open and close subject to harmonic excitations, higher harmonics generated by which can also be much less pronounced compared to the first harmonics, leading to difficulties in damage detection. Besides the detection of “breathing” cracks, the EME reported in this study can also be used for the detection of other “breathing” damage such as weak bonds or delamination by enhancing hidden higher harmonics in Q-TKEs.

Acknowledgements

This work is partially supported by the Changzhou Policy Guidance Plan-International Science and technology cooperation (No. CZ20200003). Maosen Cao and Zhongqing Su are grateful for the support from the National Natural Science Foundation of China through Grant Nos. 11772115 and 51875492, respectively. Wei Xu is particularly grateful for the fellowship provided by the Hong Kong Scholars Program (No. XJ2018042), during which he started this work.

Appendix A

The Teager-Kaiser energy of two functions a_1 and a_2 is defined as [38]

$$\begin{aligned}\psi(a_1+a_2)&=(\dot{a}_1+\dot{a}_2)^2-(a_1+a_2)(\ddot{a}_1+\ddot{a}_2)\\&=(\dot{a}_1{}^2+2\dot{a}_1\dot{a}_2+\dot{a}_2{}^2)-(a_1\ddot{a}_1+a_2\ddot{a}_2+a_1\ddot{a}_2+a_2\ddot{a}_1)\\&=(\dot{a}_1{}^2-a_1\ddot{a}_1)+(\dot{a}_2{}^2-a_2\ddot{a}_2)+(\dot{a}_1\dot{a}_2-a_1\ddot{a}_2)+(\dot{a}_2\dot{a}_1-a_2\ddot{a}_1)\\&=\psi(a_1)+\psi(a_2)+\psi_c(a_1,a_2)+\psi_c(a_2,a_1).\end{aligned} \tag{A1}$$

Therefore, one can assume $\psi(\sum_{i=1}^{n}a_i)$ $(n=2,3,...)$ to be expressed as

$$\psi(\sum_{i=1}^{n}a_i)=\sum_{i=1}^{n}\psi(a_i)+\sum_{\substack{i=1,\,j=1\\ i\neq j}}^{n}\psi_c(a_i,a_j), \tag{A2}$$

and $\psi(\sum_{i=1}^{n+1}a_i)$ can be written as

$$\begin{aligned}\psi(\sum_{i=1}^{n+1}a_i)&=\psi(\sum_{i=1}^{n}a_i+a_{n+1})\\&=\psi(\sum_{i=1}^{n}a_i)+\psi(a_{n+1})+\psi_c(\sum_{i=1}^{n}a_i,a_{n+1})+\psi_c(a_{n+1},\sum_{i=1}^{n}a_i)\\&=\left(\sum_{i=1}^{n}\psi(a_i)+\sum_{\substack{i=1,\,j=1\\ i\neq j}}^{n}\psi_c(a_i,a_j)\right)+\psi(a_{n+1})+\psi_c(\sum_{i=1}^{n}a_i,a_{n+1})+\psi_c(a_{n+1},\sum_{i=1}^{n}a_i)\\&=\left(\sum_{i=1}^{n}\psi(a_i)+\psi(a_{n+1})\right)+\left(\sum_{\substack{i=1,\,j=1\\ i\neq j}}^{n}\psi_c(a_i,a_j)+\psi_c(\sum_{i=1}^{n}a_i,a_{n+1})+\psi_c(a_{n+1},\sum_{i=1}^{n}a_i)\right)\\&=\left(\sum_{i=1}^{n}\psi(a_i)+\psi(a_{n+1})\right)+\left(\sum_{\substack{i=1,\,j=1\\ i\neq j}}^{n}\psi_c(a_i,a_j)+\sum_{i=1}^{n}\psi_c(a_i,a_{n+1})+\sum_{i=1}^{n}\psi_c(a_{n+1},a_i)\right),\end{aligned} \tag{A3}$$

in which it can be found that $\sum_{i=1}^{n}\psi(a_i)+\psi(a_{n+1})=\sum_{i=1}^{n+1}\psi(a_i)$ and $\sum_{\substack{i=1,\,j=1\\ i\neq j}}^{n}\psi_c(a_i,a_j)+\sum_{i=1}^{n}\psi_c(a_i,a_{n+1})+\sum_{i=1}^{n}\psi_c(a_{n+1},a_i)=\sum_{\substack{i=1,\,j=1\\ i\neq j}}^{n+1}\psi_c(a_i,a_j)$. Thereby, $\psi(\sum_{i=1}^{n+1}a_i)$ is expressed as

$$\psi(\sum_{i=1}^{n+1} a_i) = \sum_{i=1}^{n+1} \psi(a_i) + \sum_{\substack{i=1,j=1 \\ i \neq j}}^{n+1} \psi_c(a_i, a_j). \quad \text{(A4)}$$

Thus, Eq. (A4) is proved by recurrence method.

References:

[1] A. Israr, M. Cartmell, E. Manoach, I. Trendafilova, W. Ostachowicz, M. Krawczuk, A. Zak, Analytical modeling and vibration analysis of partially cracked rectangular plates with different boundary conditions and loading, Journal of Applied Mechanics. 76 (1) (2009) 011005.

[2] C. Wong, W. Zhang, S. Lau, Periodic forced vibration of unsymmetrical piecewise-linear systems by incremental harmonic balance method, Journal of Sound and Vibration. 149 (1) (1991) 91–105.

[3] Y. Chu, M. Shen, Analysis of forced bilinear oscillators and the application to cracked beam dynamics, AIAA Journal. 30 (10) (1992) 2512–2519.

[4] S. Chatterjee, A. Mallik, A. Ghosh, Periodic response of piecewise non-linear oscillators under harmonic excitation, Journal of Sound and Vibration. 191 (1) (1996) 129–144.

[5] A. Rivola, P. White, Bispectral analysis of the bilinear oscillator with application to the detection of fatigue cracks, Journal of Sound and Vibration. 216 (5) (1998) 889–910.

[6] S. Cheng, A. Swamidas, X. Wu, W. Wallace, Vibrational response of a beam with a breathing crack, Journal of Sound and Vibration. 225 (1) (1999) 201–208.

[7] J. Ji, C. Hansen, On the approximate solution of a piecewise nonlinear oscillator under super-harmonic resonance, Journal of Sound and Vibration. 283 (1–2) (2005) 467–474.

[8] A. Bovsunovskii, C. Surace, O. Bovsunovskii, The effect of damping and force application point on the non-linear dynamic behavior of a cracked beam at sub-

and superresonance vibrations, Strength of Materials. 38 (5) (2006) 492–497.

[9] L. Gelman, S. Gorpinich, C. Thompson, Adaptive diagnosis of the bilinear mechanical systems, Mechanical Systems and Signal Processing. 23 (5) (2009) 1548–1553.

[10] A. Chatterjee, Structural damage assessment in a cantilever beam with a breathing crack using higher order frequency response functions, Journal of Sound and Vibration. 329 (16) (2010) 3325–3334.

[11] W. Liu, M. Barkey, Nonlinear vibrational response of a single edge cracked beam, Journal of Mechanical Science and Technology. 31 (11) (2017) 5231–5243.

[12] R. Ruotolo, C. Surace, P. Crespo, D. Storer, Harmonic analysis of the vibrations of a cantilevered beam with a closing crack, Computers and Structures. 61 (6) (1996) 1057–1074.

[13] N. Pugno, C. Surace, R. Ruotolo, Evaluation of the non-linear dynamic response to harmonic excitation of a beam with several breathing cracks, Journal of Sound and Vibration. 235 (5) (2000) 749–762.

[14] K. Sholeh, A. Vafai, A. Kaveh, Online detection of the breathing crack using an adaptive tracking technique, Acta Mechanica. 188 (3–4) (2007) 139–154.

[15] A. Bouboulas, N. Anifantis, Finite element modeling of a vibrating beam with a breathing crack: observations on crack detection, Structural Health Monitoring-An International Journal. 10 (2) (2010) 131–145.

[16] P. Casini, F. Vestroni, Characterization of bifurcating non-linear normal modes in piecewise linear mechanical systems, International Journal of Non-Linear

Mechanics. 46 (1) (2011) 142–150.

[17] O. Giannini, P. Casini, F. Vestroni, Nonlinear harmonic identification of breathing cracks in beams, Computers and Structures. 129 (2013) 166–177.

[18] N. Wu, Study of forced vibration response of a beam with a breathing crack using iteration method, Journal of Mechanical Science and Technology. 29 (7) (2015) 2827–2835.

[19] F. Dotti, V. Cortínez, F. Reguera, Non-linear dynamic response to simple harmonic excitation of a thin-walled beam with a breathing crack, Applied Mathematical Modelling. 40 (1) (2015) 451–467.

[20] M. Shen, Y. Chu, Vibrations of beams with a fatigue crack, Computers and Structures. 45 (1) (1992) 79–93.

[21] A. Chasalevris, C. Papadopoulos, A continuous model approach for cross-coupled bending vibrations of a rotor-bearing system with a transverse breathing crack, Mechanism and Machine Theory. 44 (6) (2009) 1176–1191.

[22] S. Caddemi, I. Calio, M. Marletta, The non-linear dynamic response of the Euler-Bernoulli beam with an arbitrary number of switching cracks, International Journal of Non-Linear Mechanics. 45 (7) (2010) 714–726.

[23] M. Rezaee, R. Hassannejad, A new approach to free vibration analysis of a beam with a breathing crack based on mechanical energy balance method, Acta Mechanica Solida Sinica. 24 (2) (2011) 185–194.

[24] H. Lim, H. Sohn, P. Liu, Binding conditions for nonlinear ultrasonic generation unifying wave propagation and vibration, Applied Physics Letters. 104 (2014)

214103.

[25] K. Wang, M. Liu, Z. Su, S. Yuan, Z. Fan, Analytical insight into “breathing” crack-induced acoustic nonlinearity with an application to quantitative evaluation of contact cracks, Ultrasonics. 88 (2018) 157–167.

[26] A. Bovsunovsky, C. Surace, Non-linearities in the vibrations of elastic structures with a closing crack: a state of the art review, Mechanical Systems and Signal Processing. 62–63 (2015) 129–148.

[27] T. Kundu, Nonlinear Ultrasonic and Vibro-Acoustical Techniques for Nondestructive Evaluation, Springer, 2019.

[28] H. Hu, W. Staszewski, N. Hu, R. Jenal, G. Qin, Crack detection using nonlinear acoustics and piezoceramic transducers—instantaneous amplitude and frequency analysis, Smart Materials and Structures. 19 (6) (2010) 065017.

[29] F. Semperlotti, K. Wang, E. Smith, Localization of a breathing crack using super-harmonic signals due to system nonlinearity, AIAA Journal. 47 (9) (2009) 2076–2086.

[30] G. Kim, D. Johnson, F. Semperlotti, K. Wang, Localization of breathing cracks using combination tone nonlinear response. Smart Materials and Structures. 20 (5) (2011) 055014.

[31] D. Broda, L. Pieczonka, V. Hiwarkar, W. Staszewski, V. Silberschmidt, Generation of higher harmonics in longitudinal vibration of beams with breathing cracks, Journal of Sound and Vibration. 381 (2016) 206–219.

[32] K. Wang, Z. Fan, Z. Su, Orienting fatigue cracks using contact acoustic

nonlinearity in scattered plate waves, Smart Materials and Structures. 27 (9) (2018) 09LT01.

[33] E. Asnaashari, J. Sinha. Development of residual operational deflection shape for crack detection in structures, Mechanical Systems and Signal Processing. 43 (1–2) (2014) 113–123.

[34] Z. Lu, D. Dong, H. Ouyang, S. Cao, C. Hua, Localization of breathing cracks in stepped rotors using super-harmonic characteristic deflection shapes based on singular value decomposition in frequency domain, Fatigue and Fracture of Engineering Materials and Structures. 40 (2017) 1825–1837.

[35] W. Xu, Z. Su, M. Radzieński, M. Cao, W. Ostachowicz. Nonlinear pseudo-force in a breathing crack to generate harmonics, Journal of Sound and Vibration. 492 (2021) 115734.

[36] L. Cui, H. Xu, J. Ge, M. Cao, Y. Xu, W. Xu, D. Sumarac, Use of bispectrum analysis to inspect the non-linear dynamic characteristics of beam-type structures containing a breathing crack, Sensors. 21 (4) (2021) 1177.

[37] J. Kaiser, On a simple algorithm to calculate the 'energy' of a signal, International Conference on Acoustics, Speech, and Signal Processing, 1990, 381-384.

[38] J. Kaiser, Some useful properties of Teager's energy operators, IEEE International Conference on Acoustics, Speech, and Signal Processing: digital speech processing, 1993, 149-152.

[39] P. Maragos, J. Kaiser, T. Quatieri, On amplitude and frequency demodulation using energy operators, IEEE Transactions on Signal Processing. 41(4) (1993) 1532–

1550.

[40] A. Carcione, P. Blanloeuil, M. Veidt, Demodulation technique to identify nonlinear characteristics of vibro-acoustic NDT measurements, Journal of Sound and Vibration. 466 (2020) 115014.

[41] M. Cao, Z. Su, T. Deng, W. Xu, Nonlinear pseudo-force in “breathing” delamination to generate harmonics: a mechanism and application study, International Journal of Mechanical Sciences. 192 (2021) 106124.